applied sciences

MDPI

Article

Radial Point Interpolation-Based Error Recovery Estimates for Finite Element Solutions of Incompressible Elastic Problems

Nabil Ben Kahla, Saeed AlQadhi and Mohd. Ahmed *

Civil Engg. Deptt., College of Engineering, King Khalid University, Abha 61421, Saudi Arabia
* Correspondence: mall@kku.edu.sa; Tel.: +966-172418439

Abstract: Error estimation and adaptive applications help to control the discretization errors in finite element analysis. The study implements the radial point interpolation (RPI)-based error-recovery approaches in finite element analysis. The displacement/pressure-based mixed approach is used in finite element formulation. The RPI approach considers the radial basis functions (RBF) and polynomials basis functions together to interpolate the finite element solutions, i.e., displacement over influence zones to recover the solution errors. The energy norm is used to represent global and local errors. The reliability and effectiveness of RPI-based error-recovery approaches are assessed by adaptive analysis of incompressibility elastic problems including the problem with singularity. The quadrilateral meshes are used for discretization of problem domains. For adaptive improvement of mesh, the square of error equally distributed technique is employed. The computational outcome for solution errors, i.e., error distribution and convergence rate, are obtained for RPI technique-based error-recovery approach employing different radial basis functions (multi quadratic, thin-plate splint), RBF shape parameters, different shapes of influence zones (circular, rectangular) and conventional patches. The error convergence in the original FEM solution, in FEM solution considering influence-zone-based RPI recovery with MQ RBF, conventional patch-based RPI recovery with MQ RBF and conventional patch LS-based error recovery are found as (0.97772, 2.03291, 1.97929 and 1.6740), respectively, for four-node quadrilateral discretization of problem, while for nine-node quadrilateral discretization, the error convergence is (1.99607, 3.53087, 4.26621 and 2.54955), respectively. The study concludes that the adaptive analysis, using error-recovery estimates-based RPI approach, provides results with excellent accuracy and reliability.

Keywords: error estimates; effectivity; incompressibility; recovery technique; radial point interpolation; radial basis function

Citation: Kahla, N.B.; AlQadhi, S.; Ahmed, M. Radial Point Interpolation-Based Error Recovery Estimates for Finite Element Solutions of Incompressible Elastic Problems. *Appl. Sci.* **2023**, *13*, 2366. https://doi.org/10.3390/app13042366

Academic Editor: José António Correia

Received: 9 December 2022
Revised: 3 February 2023
Accepted: 9 February 2023
Published: 12 February 2023

1. Introduction

The error assessment and adaptive techniques are developed to improve the finite element analysis efficiency and to keep the discretization error within limits. The adaptive finite element technique is an iterative approach in which the finite element analysis and error estimation are first carried out, and then the solution error is checked for permissible limits, and the mesh is refined if limit is exceeded. The success of adaptive analysis depends on the accurate error estimation of selected meshing schemes. The current interest in finite element method (FEM) research is to reduce the dependency of mesh for the analysis and to develop the advanced finite element methods. Cen et al. [1] provided a review of up-to-date high-performance finite element methods including the hybrid stress-function FEM, the hybrid displacement-function FEM and the improved unsymmetric FEM, and their applications. Xu and Rajendran [2] proposed a meshfree finite element method based on partition of unity for linear and nonlinear finite element analyses. The shape-free FEM concept was proposed by Cen et al. [3], in which performances of FEM are not affected by distortion of element shapes. Three-dimensional eight-node hexahedral elements are developed by Zhou et al. [4] for resisting mesh distortion in the finite element analysis

applicable to both isotropic and anisotropic cases. They apply the virtual work principle in the development of an element considering two different sets of displacement fields that are employed simultaneously, namely traditional iso-parametric element formulations and analytical trial functions. Huang et al. [5] developed a new three-dimensional solid-shell element with mesh-resistant distortion for analysis of shells with various geometry and loading conditions. The incompressible condition of problem causes an error in analysis due to the ill conditioning of the stiffness matrix and volumetric locking. Brink and Stein [6] summarized the computational results of the approaches, namely displacement-pressure formulation, a three-field formulation and a two-field formulation based on an energy functional that deals with the incompressibility in finite element analysis. Zeng and Liu [7] used a mixed Kirchhof stress displacement-pressure formulation, Karabelas et al. [8] used a basic pressure projection stabilized method, and Doll et al. [9] use a selective-reduction integration approach to satisfy the incompressibility condition. Boffi and Stenberg [10] suggested a number of treatments for the issue of volumetric locking, which arises from the constrained nature of displacement-based finite element analysis. They consider hydrostatic pressure as unknown and satisfy the condition of the ellipticity on the kernel, in addition to the well-known Babuška–Brezzi condition. Gültekin et al. [11] employed the variational multi-scale approach-based finite element technique to investigate finite-strain incompressible elasticity with volumetric locking. The meshless method provides better accuracy than conventional FEM [12]. Guo et al. [13] proposed a universal recovery procedure to improve the accuracy of gradient approximation for virtual element methods using general polygonal meshes. Kaveh and Seddighian [14] developed the nodal stress recovery technique by fitting appropriative function using Colliding Bodies Optimization (CBO) Algorithm for nodal stress fields. The approach is a connection between analytical approaches and numerical methods, utilizing the benefits of both categories. Khan et al. [15] implemented the mixed formulations for incompressible linear elasticity problems in the finite element method. They also consider the requirement for pressure stabilization with lowest-order conforming approximations. Popișter et al. [16] developed mathematical algorithms to generate mesh using ordered/unordered point clouds, eliminating the errors which can be induced in mesh generation over the domains. Gratsch and Bathe [17] comprehensively reviewed the error estimation approaches for linear and non-linear finite element solutions. Alshoaibi and Bashiri [18] presented the adaptive modeling of crack development for linear elastic materials under fatigue conditions. The displacement projection technique was used to calculate stress-intensity factors at each crack increment. A hybrid Hermite approximation approach and an improved interpolation element-free Galerkin method is proposed by Ma et al. [19] for the analysis of elasticity problems, who found results with excellent accuracy and stability. Vogl et al. [20] conducted Zienkiewicz and Zhu error estimator-based adaptive analysis of magnetized plasma in transport-confined fusion reactors. The derivatives of field variable at the super-convergent points are used by Saikia et al. [21] to map stress field and to recover the errors in the finite element analysis by applying the artificial neural network procedure. Karvonen et al. [22] conducted probabilistic error analysis for recently proposed statistical finite element method (statFEM) based on a Gaussian process. Ahmed [23] compared the recently proposed influence-zones-based error-recovery techniques including RPI method for elastic finite element solutions. Gong et al. [24] developed an interface model of soil and structure employing the radial point interpolation approach in finite element method. A hybrid approach using element-free Galerkin (EFG) and radial point interpolation (RPI) technique was developed by Cao et al. [25] to deal with the imposition of displacement boundary conditions of the elastic problems.

It is clear from the survey of the relevant literature that the recent research interest in FEM is to reduce the dependency of the mesh for the analysis, and also to increase the effectivity of the finite element solution errors. Thus, error-recovery techniques in a mesh-free environment need to be further developed particularly for adaptive finite element analysis of large deformation or incompressibility problems. The present study proposes

the mesh-free RPI-based error recovery for finite element analysis of incompressible-elastic problems. The displacement-pressure-based mixed approach is employed in finite element formulation. The elastic plate examples with a known analytical solution are analyzed to investigate the performance of RPI-based error recovery in terms of the error properties, i.e., convergence rate, distribution and effectivity. The four-node quadrilateral meshing is used for domain discretization. The effect of influence-zone type, namely circular and rectangular zones of influence, and RBF types, namely MQ and TSP radial basis function, along with their shape parameters, is also investigated in RPI-based error-recovery analysis. The RPI-based error-recovery technique performance is compared with least-square (LS)-based error-recovery technique on the conventional patches. The conventional patch contains the union of the surrounding elements around the particular element [26]. The incompressible-elastic finite element formulation and finite element error estimation procedure are given in Appendix A.

2. Radial Point Interpolation (RPI) Technique-Based Error Recovery

The radial point interpolation (RPI) technique takes into account both the polynomials basis function (PBF) and radial basis functions (RBF) for interpolation [27]. Consider a problem domain Ω. To approximate a function u(x) in Ω, the node interpolant $u^h(x)$ is defined in domain Ω by

$$u^h(x) = \sum_{i=1}^{n} B_i(r)\, a_i + \sum_{j=1}^{m} p_j(x) b_j(x) \tag{1}$$

with the constraint condition

$$\sum_{i=1}^{n} p_{ij}(x) a_i = 0,\ j = 1 - m, \tag{2}$$

where $B_i(r)$ is the radial basis functions, n is the number of nodes in the neighborhood of x, $p_j(x)$ is the monomial in the space coordinates $x^T = [x, y]$, and coefficient a_i and b_j are the interpolant constant m is the number of polynomial basis function.

In the radial basis function $B_i(r)$, the variable is only the distance, r, between the interpolation node **x** and a node $\mathbf{x}_i$. For a two-dimensional problem, r is defined as

$$r = [(x_j - x_i)^2 + (y_j - y_i)^{0.5}] \tag{3}$$

There are a number of radial basis functions. The multi-quadrics (MQ) radial function and thin-plate splint radial basis function (TPS) are used in the present study. It has been proved that this term can improve interpolation accuracy. In Equation (1), only limited number $p_j(x)$ is sufficient, i.e., m << n. The following linear polynomial basis is employed.

$$P^T(x) = [1\ x\ y], \tag{4}$$

The coefficient a_i and b_j in Equation (1) can be determined by enforcing Equation (1) to be satisfied at the n nodes surrounding node x. Equation (1) can be rewritten in matrix form as

$$\begin{bmatrix} u \\ 0 \end{bmatrix} = \begin{bmatrix} B_0 & P \\ P^T & 0 \end{bmatrix} \begin{bmatrix} a \\ b \end{bmatrix} = \mathrm{G}\ a_0 \tag{5}$$

where

$$P^T = \begin{bmatrix} 1 & 1 & -- & 1 \\ x_1 & x_2 & -- & x_n \\ y_1 & y_2 & -- & y_n \end{bmatrix} \tag{6}$$

$$B_0 = \begin{bmatrix} B_1(r_1) & B_2(r_1) & - & B_n(r_1) \\ B_1(r_2) & B_2(r_2) & - & B_n(r_2) \\ - & - & -- & - \\ B_1(r_n) & B_2(r_n) & -- & B_n(r_n) \end{bmatrix} \tag{7}$$

$$a_0^T = [a_1,\ a_2, - - - - - - - - a_n,\ b_1, b_2,\ b_3] \tag{8}$$

Hence, we have

$$u(x) = \Phi(x)\ u_e, \tag{9}$$

where the shape function $u(x)$ is defined by

$$\Phi(x)\ =\ \left[B_1(r)\quad B_2(r) - - - B_n(r)\ \ 1\quad x\quad y\right] G^{-1} \tag{10}$$

and

$$u_e^T = [u_1,\ u_2, - - - - - - - - u_n,\ 0\quad 0\ \ 0] \tag{11}$$

The shape function $\Phi(x)$ obtained through the above procedure possesses delta function properties, i.e.,

$$\varnothing_i(x_j) = \delta_{ij} = \begin{Bmatrix} 1, & i = j \\ 0, & i \neq j \end{Bmatrix} \tag{12}$$

2.1. Multi-Quadrics Radial Basis Function (MQ)

There are a number of radial basis functions. and the radial basis function (RBF) affects the performance of RPI procedure considerably. The RBF multi-quadrics (MQ) with dimensionless coefficient (α_0) is formulated as

$$R_i(x_j) = [(x_j - x_i)^2 + (y_j - y_i)^2 + (\alpha_0\_d_c)^2]^q,\ \alpha_0 \geq 0 \tag{13}$$

where d_c = characteristic length relating the nodal distance of the point x (smallest distance between the node i and nodes in influence zones).

2.2. Thin-Plate Splint Radial Basis Function (TPS)

Thin-plate splint RBF is formulated as follows:

$$R_i(x_j) = \{[(x_j - x_i)^2 + (y_j - y_i)^2]\}^{\eta/2}, \tag{14}$$

The α_0, q and η are the radial basis functions shape parameters. In employing radial basis functions, the shape parameters must be identified for optimal performance. It was found from the earlier study [28] that for two-dimensional elastic plate problem using multi-quadrics RBF and errors measured in energy norm, $\alpha_0 = 5.0$ and $q = 1.03$ perform well, and the same are adopted in this study The value of η is taken as four (4) with thin-plate splint RBF. For a plate problem with rigid inclusion, the value of α_0 and q are taken as 10.0 and 1.03 for multi quadrics RBF in RPI-based error recovery.

In Equation (1), the linear polynomial added into the RBF can ensure linear consistency and improve accuracy [29]. The linear polynomial basis having m as 3 is used, and is given below as

$$p^T(x_i) = [1, x_i, y_i,], \tag{15}$$

The mesh-free interpolation performance depends on the selection of influence-zone types. The influence zones of a circular shape are formed from the distance d (= $\| x - x_i \| / d_m$). The $(x - x_i)$ is the distance from node x to point x_i, and d_m is the size of the influence zone of the point x_i; the influence size of the ith node, d_{mi}, is calculated by $d_{mi} = d_{max}\ c_i$, in which d_{max} is a dilation parameter. The distance c_I is calculated by probing for sufficient neighbor nodes distance. In this study, the value of d_{max} is assumed as 3.0. For regularly distributed nodes, c_i is simply the distance between two neighboring nodes, while for irregularly distributed nodes, c_i can be taken as an average distance of nodes in the influence zone of x_i. For the construction of influence zones of rectangular shape, the distance along two cartesian directions are $r_x = \|x - x_i\| / d_{mx}$ and $r_y = \|y - y_i\| / d_{my}$, where $d_{mx} = d_{max}\ c_{xi}$ and $d_{my} = d_{max}\ c_{yi}$. For uniformly distributed nodes, c_i is simply the distance between two neighboring nodes. For non-uniformly distributed nodes, c_i can be taken as an average nodal spacing in the support domain of x_i.

The PIM-based error-recovery technique and error estimators directed mesh updating schemes are implemented in 2D-finite element computer software. The program is also incorporated with standard patch least-square error-recovery technique and incompressible-elasticity formulation. The software is installed on intel core i7 computer with 2.6 GHz processor and 16 GB RAM to analyze the incompressible-elastic problems. Figure 1 depicts the error-recovery approach coupled with the adaptive incompressible-elastic finite-element analysis flow chart.

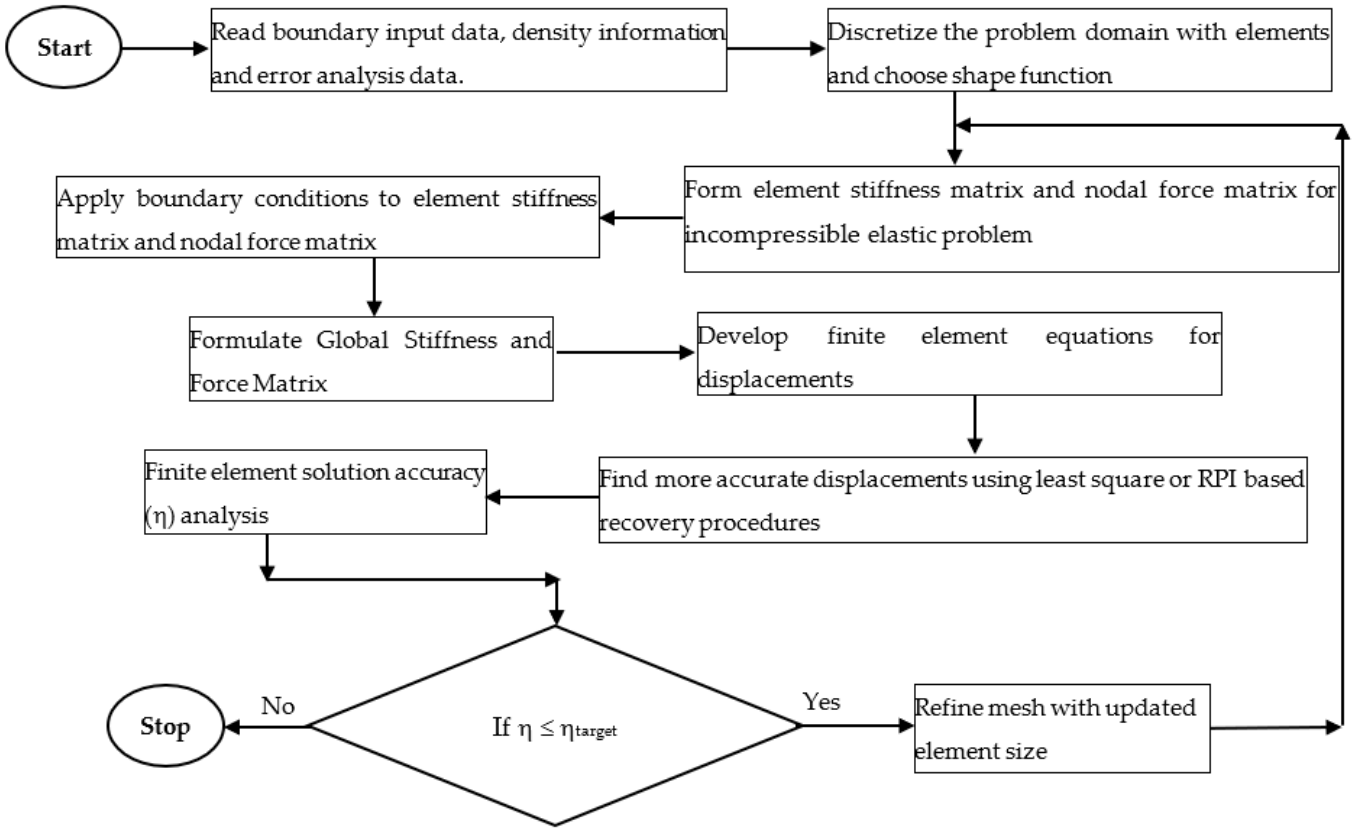

Figure 1. Flow chart for adaptive finite element analysis of the incompressible-elasticity problem using least-square and RPI-based recovery techniques.

3. Applications to Benchmark Examples

3.1. Incompressible-Elastic Square Plate

A convergence study of the recovery of errors in displacement or stress for an incompressible-elastic problem subjected to self-weight is used to test the effectiveness of the RPI-based error-recovery scheme. This problem is employed by Zienkiewicz et al. [30]. The absence of singularity in the illustrative plate problem enables the theoretical convergence rate of the ZZ recovery scheme to be compared to that of alternative recovery schemes. The analytical solutions for the illustrative plate problem are given in Equations (16)–(20).

Domain and Boundary Conditions: Ω [1, 1], $u = v = 0$ on Γ.

Analytical Solutions:

$$u = 2x^2\, y(1-x)^2(1-y)(1-2y), \tag{16}$$

$$v = -2x\, y^2\, (1-x)(1-2x)\, (1-y)^2, \tag{17}$$

$$p = x^2 - y^2, \tag{18}$$

Body Self-weight:

$$b_x = 4y\left(1-6x+6x^2\right)\left(1-3y+2y^2\right)+12x^2\left(1-2x+x^2\right)(-1+2y)-2x, \quad (19)$$

$$b_y = -4x\left(1-6y+6y^2\right)\left(1-3x+2x^2\right)+12y^2\left(1-2y+y^2\right)(-1+2x)+2y, \quad (20)$$

The adaptive analysis of the illustrative plate problem is carried taking four-node quadrilateral elements with one-point reduced integration and nine-node quadrilateral elements with four-point reduced integration for volumetric strain term (Figure 2). The target error in energy norm is kept as 2%. The computational results for error properties with various recovery procedures in energy norms considering influence zones and conventional patches are tabulated in Tables 1–3.

Figure 2. Regular and irregular quadrilateral meshing schemes.

Table 1. Error properties results for LS- and RPI (MQ)-based recovery approach in incompressible-elastic plate analysis considering influence zones and conventional patches (four-node quadrilateral regular mesh).

Mesh Size (1/h)	FEM Error ($\times 10^{-3}$)	RPI (Influence Zone, MQ)		RPI (Conventional Patch, MQ)		LS (Conventional Patch)	
		Error ($\times 10^{-3}$)	Effectivity	Error ($\times 10^{-3}$)	Effectivity	Error ($\times 10^{-3}$)	Effectivity
1/4	29.44	8.30	0.96649	10.21	0.79000	15.95	0.90074
1/16	7.69	0.49	1.00823	0.72	0.98241	1.79	1.00184
1/32	3.85	0.12	1.00364	0.17	0.99637	0.49	1.00092
Conv. Rate	0.97772	2.03291		1.97929		1.67400	

Table 2. Error properties results for LS- and RPI (MQ)-based recovery approach in incompressible-elastic plate analysis considering influence zones and conventional patches (nine-node quadrilateral regular mesh).

Mesh Size (1/h)	FEM Error ($\times 10^{-3}$)	RPI (Influence Zone, MQ)		RPI (Conventional Patch, MQ)		LS (Conventional Patch)	
		Error ($\times 10^{-3}$)	Effectivity	Error ($\times 10^{-3}$)	Effectivity	Error ($\times 10^{-3}$)	Effectivity
1/4	4.44	0.580	1.13369	6.927	1.87269	2.757	1.04939
1/8	1.11	0.054	1.19421	0.081	0.98104	0.702	1.01182
1/16	0.279	0.017	1.00075	0.018	0.99259	0.021	1.00111
Conv. Rate	1.99607	3.53087		4.26621		2.54955	

Table 3. Error properties results for LS- and RPI (MQ)-based recovery approach in incompressible-elastic plate analysis considering influence zones and conventional patches (four-node quadrilateral irregular mesh).

Mesh Size		FEM Error ($\times 10^{-3}$)	RPI (Influence Zone, MQ)		RPI (Conventional Patch, MQ)		LS (Conventional Patch)	
			Error ($\times 10^{-3}$)	Effectivity	Error ($\times 10^{-3}$)	Effectivity	Error ($\times 10^{-3}$)	Effectivity
30	82	31.69	25.04	0.83372	25.05	0.79958	23.04	0.80883
615	1218	5.39	1.89	0.98982	1.96	0.99366	1.33	0.99778
2598	5798	2.73	0.86	0.98908	0.89	0.99317	0.57	1.00702

3.1.1. Effect of Influence-Zone Shape and Radial Basis Function and Its Shape Parameters in RPI-Based Error Recovery

In order the study the shape of influence zone and RBI in RPI-based recovery, the rectangular influence-zone shape (Figure 3) and thin-plate splint (TPS) RBI are also considered in incompressible-elastic finite element analysis. The influence of the shape parameters value of η =5 for TPS RBI is also studied. The computational results for RPI interpolation considering circular/rectangular zones and conventional patch with thin-plate splint (TPS) RBI and shape parameters are given in the following Tables 4–6 for regular and irregular mesh of quadrilateral elements.

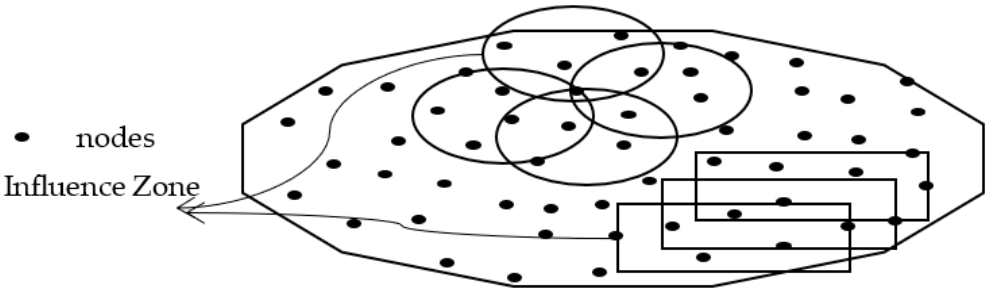

Figure 3. Influence zones for RPI-based error-recovery technique.

Table 4. Error properties results for RPI (TPS)-based recovery techniques in incompressible-elastic plate analysis considering influence zones and conventional patches (four-node quadrilateral regular mesh).

Mesh Size (1/h)	FEM Error ($\times 10^{-3}$)	RPI (Circular Influence Zone, TPS, η = 4)		RPI (Conventional Patch, TPS, η = 4)		RPI (Rectangular Influence Zone, TPS)	
		Error ($\times 10^{-3}$)	Effectivity	Error ($\times 10^{-3}$)	Effectivity	Error ($\times 10^{-3}$)	Effectivity
1/4	29.44	13.16	0.96649	12.31	0.79461	13.29	0.83386
1/16	7.69	0.901	1.00823	0.914	0.98862	0.796	0.97836
1/32	3.85	0.234	1.00364	0.204	0.99450	0.161	0.99601
Conv. Rate	0.97772	1.93875		1.97230		2.12271	

Table 5. Error properties results for RPI (TPS)-based recovery techniques in incompressible-elastic plate analysis considering influence zones and conventional patches (four-node quadrilateral irregular mesh).

Mesh Size		FEM Error ($\times 10^{-3}$)	RPI (Circular Influence zone, TPS, η = 4)		RPI (Conventional Patch, TPS, η = 4)		RPI (Rectangular Influence Zone, TPS)	
			Error ($\times 10^{-3}$)	Effectivity	Error ($\times 10^{-3}$)	Effectivity	Error ($\times 10^{-3}$)	Effectivity
30	82	31.691	25.28	0.82779	25.017	0.79698	24.681	0.85763
615	1218	5.387	1.818	0.97268	1.900	0.98447	1.929	0.98678
2598	5798	2.732	0.852	0.98871	0.889	0.99513	0.907	0.99393

Table 6. Error properties results for RPI (TPS)-based recovery techniques in incompressible-elastic plate analysis considering TPS RBF shape parameter and conventional patches (four-node quadrilateral regular mesh).

Mesh Size (1/h)	FEM Error ($\times 10^{-3}$)	RPI (Circular Influence Zone, TPS, η = 5)		RPI (Conventional Patch, TPS, η = 5)	
		Error ($\times 10^{-3}$)	Effectivity	Error ($\times 10^{-3}$)	Effectivity
1/4	29.44	13.31	0.80100	11.31	0.85831
1/16	7.69	1.488	0.95403	1.204	0.98862
1/32	3.85	0.698	0.96364	0.555	0.94069
Conv. Rate	0.97772	1.41784		1.46772	

3.1.2. Finite Error Distribution in Plate Domain

The error distribution pattern is replicated in adaptively improved meshes that result from adaptive analysis to obtain a target error limit throughout the problem domain. The finite element analysis in adaptive environment incorporating the RPI-based error recovery is carried out to target error limit of 4%. Table 7 shows the adaptive analysis results (overall error, total number of elements and degree of freedom (DOF)) for a target error limit of 4% with quadrilateral discretization using the RPI error recovery employing multi-quadrics (MQ)/thin-plate splint (TPS) RBF, circular/rectangular influence-zones shapes and conventional patches. Figure 4 depicts the plots of adaptive refined meshes obtained from adaptive analysis employing radial point interpolation-based error recovery using multi-quadrics (MQ) and thin-plate splint (TPS) RBF, circular and rectangular influence-zones shapes, and conventional patches.

Table 7. Adaptive finite element analysis results (overall errors, total number of elements (N) and DOF) for incompressible-elastic plate with 4% target error using quadrilateral elements.

Recovery Type	Adaptive Analysis Results (Original Uniform Mesh with 615 Elements and 1218 DOF, 4% Target Error)			
	FEM Error	Projected Error	Adaptive Mesh Properties	
			N	DOF
LS (conventional patches)	9.43	9.64	5629	11,520
RPI (influence zones-MQ-Cir.)	9.43	9.26	5872	12,026
RPI (conventional patches-MQ)	9.43	9.30	5606	11,490
RPI (influence zones-TSP-Cir.)	9.43	9.13	5950	12,086
RPI (influence zones-TSP-Rect.)	9.43	9.22	5454	11,186
RPI (conventional patches-TSP)	9.43	9.23	5587	11,454

3.2. Infinite Incompressible-Elastic Plate with Rigid Circular Opening

The infinite incompressible-elastic plate with circular opening example is also analyzed to examine the recovery properties of the mesh-free RPI-based recovery schemes. The adaptive mesh-refining approach is implemented to study the error distribution behavior. The analytical solution of the example problem is known [31]. The gradients are continuous on both the boundary and inside domain, having one or more singular points outside of the domain. The following equations can be used to obtain true displacement and stresses in the problem.

$$u_r = \left(\frac{T_x}{8Gr}\right)\{(k-1)r^2]+2\gamma R^2+[\beta(k-1)R^2+2r^2-2\delta\left(\frac{R^4}{r^2}\right)]\}\ cos2\theta, \quad (21)$$

$$u_\theta = -\left(\frac{T_x}{8Gr}\right)\left[\beta(k-1)R^2+2r^2-2\delta\left(\frac{R^4}{r^2}\right)\right]sin2\theta, \quad (22)$$

$$\sigma_{rr} = (T_x/2)\left[1-\gamma\left(R^2/r^2\right)\right]\ ]+(T_x/2)\ [1-2\beta\left(R^2/r^2\right)+3\delta\left(R^4/r^4\right)\ cos2\theta, \quad (23)$$

$$\sigma_{\theta\theta} = \left(\frac{T_x}{2}\right)\left[1+\gamma\left(\frac{R^2}{r^2}\right)\right]-(T_x/2)\ \left[1-3\delta\left(R^4/r^4\right)\right]\ cos2\theta\ , \quad (24)$$

$$\tau_r = -(T_x/2)\ \left[1+\beta\left(\frac{R^2}{r^2}\right)+3\delta\left(R^4/r^4\right)\right]\ sin2\theta, \quad (25)$$

where $r = y^2 + \underline{x^2}$, T_x = uniaxial traction applied at infinity, and constants k[=3 − 4υ], β[=−2/(3 − 4υ)], γ[=−(2 − 4υ)/2], δ[=1/(3 − 4υ)] depend on Poisson's ratio υ only.

The dimensions of the problem are taken as R = 1 unit, $w = b$ = 4 unit, as shown in Figure 5. The rigid circular opening's center is a singular point. Both of the displacement components have a value of zero along the edge of the circular arc AE. Both the normal displacement

component and the shear stress are equal to zero along the CB and DE border symmetry lines. Along boundaries AB and CD, the tractions computed from Equations (23)–(25) are imposed. The numerical quadrature using 12- Gauss points per element side is used to calculate the corresponding load vectors. The plate problem is analyzed by RPI-based error estimator incorporated adaptive procedures and the target error in energy norm is kept as 2%. The uniform subdivision of four-node quadrilateral elements is used. The discretized domain is shown in Figure 5. The numerical results of the convergence of error and effectivity for four-node quadrilateral elements with one-point reduced integration for penalty term is given in Table 8. The adaptive mesh refinement results, i.e., degrees of freedom (DOF) and number of element (N) after mesh was updated for 2% target error in incompressible plate with rigid circular opening, considering meshless and conventional patches are given in Table 9. The updated mesh plots for target error of 2% are depicted in Figure 5.

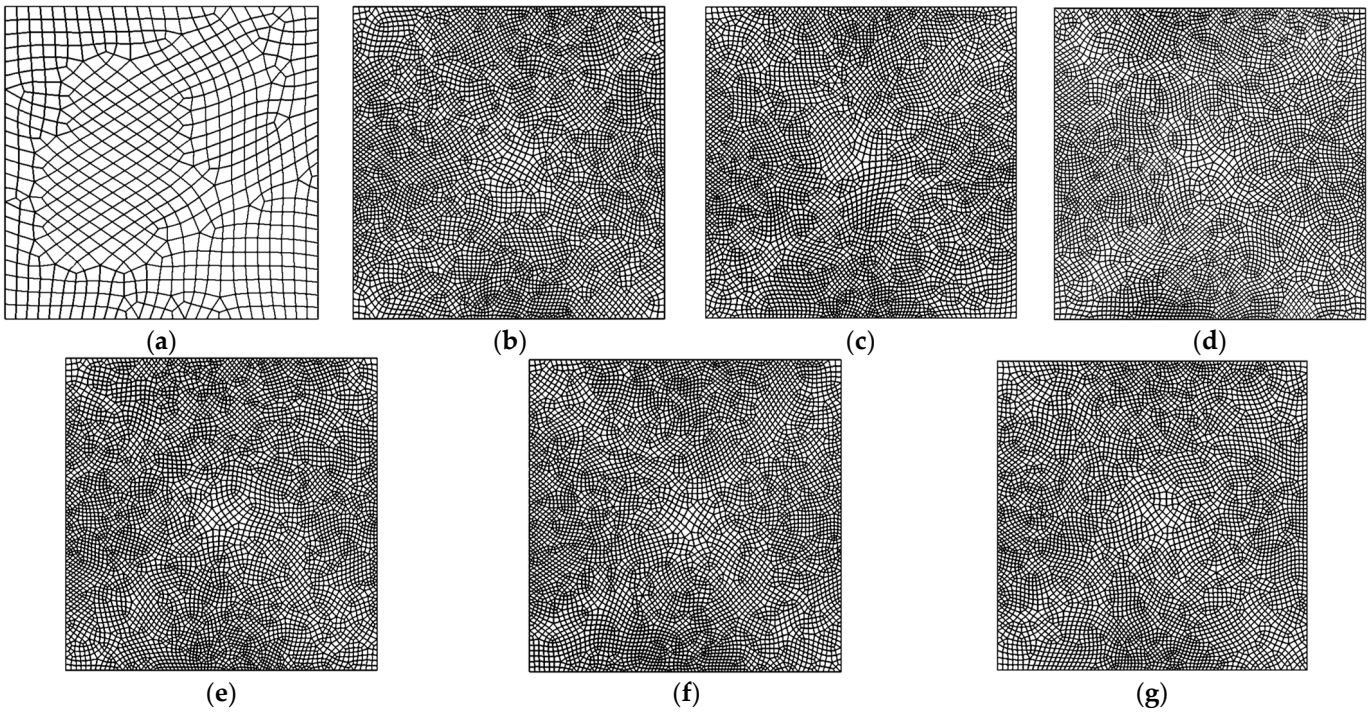

Figure 4. Refined mesh plots in incompressible plate with RPI-recovery techniques considering influence zones and conventional patches (quadrilateral elements original mesh = 30, 4% target accuracy). (**a**) Mesh (original). (**b**) LS (conventional patch, ZZ). (**c**) RPI (conventional patch, MQ). (**d**) RPI (conventional patch, TSP). (**e**) RPI (influence zones, MQ, cirular). (**f**) RPI (influence zones, TSP, cirular). (**g**) RPI (influence zones, TSP, rectangular).

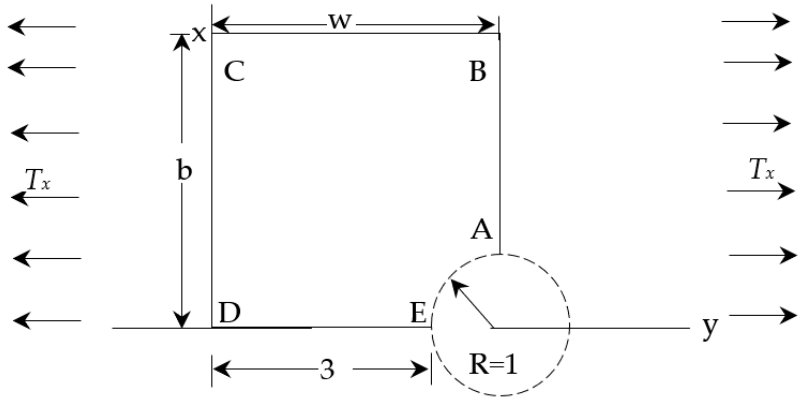

Figure 5. Plate with rigid circular opening.

Table 8. Error properties found for LS- and RPI (MQ)-based recovery approach in incompressible-elastic analysis for plate with rigid circular opening considering influence zones and conventional patches. (Four-node quadrilateral equal elements).

Mesh Size		FEM Error	RPI (Influence Zone, MQ)		RPI (Conventional Patch, MQ)		LS (Conventional Patch)	
			Error	Effectivity	Error	Effectivity	Error	Effectivity
233	534	0.1680	0.1071	0.88526	0.1148	0.81606	0.1177	1.03672
793	1698	0.0912	0.0584	0.98995	0.0604	0.98564	0.0516	1.02639
2467	5130	0.0546	0.0266	0.95198	0.0272	0.94467	0.0234	0.97784

Table 9. Adaptive finite element analysis results (errors, total number of elements (N) and DOF) for incompressible-elastic plate with 2% target error using quadrilateral elements.

Recovery Type	Adaptive Analysis Results (Original Uniform Mesh with 233 Elements and 534 DOF, 2% Target Error)			
	FEM Error	Projected Error	Adaptive Mesh Properties	
			N	DOF
LS (conventional patch)	4.93	5.12	739	1586
RPI (Meshfree-MQ-Cir.)	4.93	9.35	291	652
RPI (conventional patch-MQ)	4.93	4.02	346	770

4. Discussion

The study implements the RPI-based error-recovery approaches in finite element error analysis. The displacement/pressure-based mixed approach is used in finite element formulation. The accuracy and reliability of RPI-based error-recovery approaches is assessed for incompressibility-elastic problem. The adaptive analysis computational results are obtained for error quality, i.e., errors convergence, effectivity with increasing order of fineness and refined meshes for target error, by simulating the incompressible plate benchmark examples. The problem domain is meshed using 4/9 node quadrilateral elements. The target error in energy norm for four-node elements is kept as 4% in incompressible-elastic plate and 2% for incompressible-elastic plate with rigid circular opening. The incompressible-elastic analysis results for plate problems in terms of convergence of error, effectivity for least-square and radial point interpolation-based recovery procedures using influence zones/standard patches, and MQ/TSP radial basis function and two-shape parameter value (η =4, 5) are tabulated in Tables 1–9.

From Tables 1–6, it is clear that the error convergence obtained with the help of the RPI recovery is found to be better than that for the least-square error-recovery technique. The performance of RPI influence-zone-based recovery is better as compared to conventional patches-based radial-point interpolation error recovery. This may be due to inaccurate recovery for nodes on boundary since fewer nodes are available. The influence-zone-based recovery technique eliminates such difficulties. The order of error is also smaller in RPI error recovery, thereby indicating higher efficiency of the RPI-based error-recovery technique. The higher order quadrilateral elements also present similar error properties results for RPI error-recovery-based adaptive finite-element analysis. However, error convergence in conventional patch-based RPI error-recovery technique is higher compared to influence-zone-based RPI error-recovery technique. The convergence of errors in the original finite element solution, and in the solution employing circular influence-zone-based RPI recovery with MQ RBF, conventional patch-based RPI recovery with MQ RBF and conventional patch-based least-square (LS) error recovery, are found as (0.97772, 2.03291, 1.97929 and 1.6740) and (1.99607, 3.53087, 4.26621 and 2.54955), respectively, for four-node and nine-node quadrilateral discretization of elastic plate problem. The performance of RPI-based error-recovery approach is also investigated for the plate problem with circular opening. It is evident from the Tables 7 and 8 and Figure 6 that computation results of influence-zone-

based RPI-recovery approach have higher global effectivity than the conventional patch-based LS error-recovery approach, with more optimize error distribution characteristics.

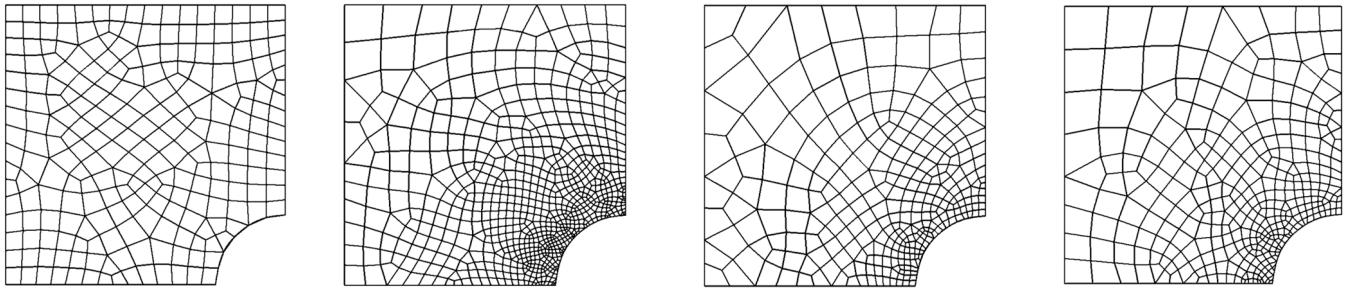

Figure 6. Refined mesh plots of incompressible plate having rigid circular opening with RPI-recovery techniques considering influence zones and conventional patches (quadrilateral elements original mesh =233, 2% target accuracy). (**a**) Mesh (original). (**b**) LS (conventional patch). (**c**) RPI (influence zones, MQ, cirular). (**d**) RPI (conventional patch, MQ).

The effect of influence-zone type, namely circular and rectangular zones of influence, and RBF type, namely MQ and TSP radial basis function, is also investigated in RPI-based error-recovery analysis. The results indicated that influence-zone and RBF type affect considerably the error quality and effectivity in RPI-based error-recovery analysis. The rectangular zone of influence improves the error convergence and reduces the order of error, while performance of TSP radial basis function is better than the MQ radial basis function in RPI-based error recovery in incompressible-elastic problem. The error convergences' infinite element solutions using circular and rectangular influence-zone-based RPI recovery with TSP RBF are 1.93875 and 2.12271. The optimal value of the shape parameter (η) of TSP radial basis function is four (4), as by increasing the η value, the order of error increases and rate of error convergence decreases.

The error distribution pattern is replicated in adaptively improved meshes that resulted from adaptive analysis to obtain a target error limit throughout the problem domains. The adaptive analysis incorporating the error recovery based on RPI is carried out for target error limits of 4% and 2%, respectively, for square plate and plate with rigid circular opening. The degrees of freedom and total number of elements (N) after mesh updated for target error with RPI-recovery techniques using quadrilateral discretization are presented in Tables 6 and 8. The updated mesh plots for the target error obtained in RPI-recovery techniques considering influence zones/standard patches and MQ/TSP radial basis function are shown in Figures 4 and 6. It is observed from the updated meshes that the RPI error computation is more efficient as compared to the standard patch-based error computation. It can be concluded that the adaptive analysis using radial-point interpolation-based error-recovery estimation provides results with excellent accuracy and reliability.

5. Conclusions

The study implements the radial point interpolation (RPI)-based error-recovery approaches in finite element analysis. The displacement/pressure-based mixed approach is used in finite element formulation. The solution errors are quantified in energy norms. The reliability and effectiveness of RPI-based error-recovery approaches is assessed by the adaptive analysis of the incompressibility elastic problem including the problem with singularity. The quadrilateral meshes are used for discretization of problem domains. The square of error equally distributed scheme is used for adaptive improvement of mesh. The computational outcome for solution errors, i.e., error distribution and convergence rate, are obtained for RPI technique-based error-recovery approach with multi quadratic/thin-plate-splint radial basis functions, circular/rectangular influence zones and conventional patches. The error convergence obtained with the help of RPI recovery is found to be better than

that for the least-square error-recovery technique. The performance of RPI influence-zone-based recovery is better as compared to conventional patches-based RPI error recovery. It is observed that influence-zone and RBF type affect considerably the error quality and effectivity in RPI-based error-recovery analysis. The rectangular zone of influence improves the error convergence and reduces the order of error, while performance of TSP radial basis function is better than the MQ radial basis function in RPI-based error recovery in the incompressible-elastic problem. It can be concluded that the adaptive analysis under the guidance of radial point interpolation-based error-recovery estimation provides results with excellent accuracy and reliability.

Author Contributions: Conceptualization, M.A.; methodology, N.B.K.; validation, N.B.K. and S.A.; formal analysis, M.A. and S.A.; investigation, N.B.K.; resources, N.B.K.; writing—original draft preparation, M.A.; writing—review and editing, N.B.K. visualization, S.A.; supervision S.A.; project administration, S.A.; funding acquisition, M.A. All authors have read and agreed to the published version of the manuscript.

Funding: This research was funded by Deanship of Scientific Research at King Khalid University for funding this work through Large Group Research Project under grant number (R.G.P2 /190/43).

Institutional Review Board Statement: Not applicable.

Informed Consent Statement: Not applicable.

Data Availability Statement: Not applicable.

Acknowledgments: The authors extend their appreciation to the Deanship of Scientific Research at King Khalid University for funding this work through Large Group Research Project under grant number (R.G.P2 /190/43). The authors also acknowledge to the Dean, Faculty of Engineering for his valuable support and help.

Conflicts of Interest: The authors declare no conflict of interest. The funders had no role in the design of the study; in the collection, analyses, or interpretation of data; in the writing of the manuscript, or in the decision to publish the results.

Appendix A

Appendix A.1 Finite Element Formulation for Incompressible Elasticity [30]

The momentum balance equation and incompressibility constraints in the incompressible elastic formulation are given as follows,

$$\mathrm{L}^{T}\sigma + f = 0 \; in \; \Omega, \tag{A1}$$

$$\nabla^{T} u = m^{T} L \, u = 0 \; in \; \Omega \, , \tag{A2}$$

$$\sigma \, n = \bar{t} \; on \; \Gamma_t, \text{and} u = \overline{u} \; on \; \Gamma_u \tag{A3}$$

where Ω is a problem domain, f is body forces σ ε and u are the stress, strain and displacement in body.

The displacement-pressure mixed formulation is used for the analysis. The constitutive relation can be written as,

The stress (σ) and strain (ε) relation for mixed formulation in terms of displacement (u) and pressure (p) can be written as,

$$\sigma = 2\mu\left(\varepsilon - \frac{1}{3}\mathrm{mm}^{\mathrm{T}}\varepsilon\right) + \mathrm{m}p, \text{ or} \tag{A4}$$

where m^{T} = [1,1,1, 0, 0, 0], σ is the stress tensor, ε is the strain tensor, u is the displacement and L defines the strain as

$$\varepsilon = Lu, \tag{A5}$$

Approximating independently u and p by $u = \mathrm{N}_u\overline{u}$, and $p = \mathrm{N}_p\overline{p}$, and performing the Galerkin approximation, we have the discretized system of equations

$$p = \mathrm{N}_p\overline{p}\,, \tag{A6}$$

$$\begin{bmatrix} A & B \\ B^T & 0 \end{bmatrix} \begin{Bmatrix} \overline{u} \\ \overline{p} \end{Bmatrix} = \begin{bmatrix} f_1 \\ f_2 \end{bmatrix} \tag{A7}$$

where $B = \int_\Omega G^T m N_P d\Omega$, $A = \int_\Omega G^T 2\mu\left(I - \frac{1}{3}\mathrm{mm}^T\right) G d\Omega$,

$$\mathbf{f}_1 = \int_{\Gamma_i} \mathbf{N}_\mathbf{u}^\mathbf{T} \bar{\mathbf{t}}_\mathbf{i} \mathbf{d}\Gamma + \int_\Omega \mathbf{N}_\mathbf{u}^\mathbf{T} \mathbf{f}\ \mathbf{d}\Omega$$

$$\mathbf{G} = \mathbf{L}\mathbf{N}_\mathbf{u},\ f_2\ =\ 0$$

Appendix A.2 FiniteElement Errors and Adaptivity [26]

The finite element errors are the deviation of the original finite element results from the recovered results (or exact results). Solution errors are evaluated in in scalar quantity terms i.e., energy norms or L_2 norms. The reliability of error estimations is measured in terms of effectivity. The ratio between the projected error and the exact error i.e., effectivity (θ), provide the reliability of the error estimators.

$$\theta = \frac{\|e\|}{\|e_{ex}\|} \tag{A8}$$

where $\|e\|_E (= \left[\int_\Omega e_\sigma^{*T} D^{-1} e_\sigma^* d\Omega\right]^{\frac{1}{2}})$ represent the evaluated error, and $\|e_{ex}\|_E$ is the exact error (in energy norms), D is the elasticity matrix.

Solution accuracy (η) in finite element analysis is given as follows.

$$\eta = \frac{\|e\|}{\|\sigma^*\|} \tag{A9}$$

where $\|\sigma^*\|^2 = \|\sigma^h\|^2 + \|e\|_E{}^2$, $\|\sigma^h\| (= \left[\int_\Omega \sigma^T D^{-1} \sigma^T d\Omega\right]^{\frac{1}{2}})$.

The finite element solution is accepted when target accuracy (η_{target}) is more than the accuracy (η) of the solution. The mesh may be improved in adaptive way i.e., only on locations where the errors are more than the target error. The global target error is calculated as follows.

$$\|e\|_{target} = \eta_{target} \|e\| / k \tag{A10}$$

where k is a factor lying between 1.0 to 1.5 to avoid oscillation [32].

The target error in the ith element is calculated using the following equation [26].

$$\frac{\|e\|_{target\ (i)}}{\sqrt{\Omega_i}} = \frac{\|e\|_{target}}{\sqrt{\Omega}} \tag{A11}$$

where Ω is the volume of the domain, Ω_i is the volume of the ith element.

Mesh improvement parameter (ξ_i) that directs mesh refining is as follows.

$$\xi_i = \frac{\|e\|_{target}}{\|e\|_{target\ (i)}} \tag{A12}$$

The mesh improvement is required when element improvement parameter is greater than one. The updated mesh size ($h_{updated}$) can be found as.

$$h_{updated} = \frac{h_{old}}{\xi_i^{1/p}} \tag{A13}$$

where p is the order of the approximating polynomial and h_{old} is the old size of the ith element.

References

1. Cen, S.; Wu, C.J.; Li, Z.; Shang, Y.; Li, C. Some advances in high-performance finite element methods. *Eng. Comput.* **2019**, *36*, 2811–2834. [CrossRef]
2. Xu, J.P.; Rajendran, S. A 'FE-Meshfree' TRIA3 element based on partition of unity for linear and geometry nonlinear analyses. *Comput. Mech.* **2013**, *51*, 843–864. [CrossRef]
3. Cen, S.; Fu, X.R.; Zhou, M.J. 8- and 12-node plane hybrid stress-function elements immune to severely distorted mesh containing elements with concave shapes. *Comput. Methods Appl. Mech. Eng.* **2011**, *200*, 2321–2336. [CrossRef]
4. Zhou, P.L.; Cen, S.; Huang, J.B.; Li, C.F.; Zhang, Q. An unsymmetric 8-node hexahedral element with high distortion tolerance. *Int. J. Numer. Methods Eng.* **2017**, *109*, 1130–1158. [CrossRef]
5. Huang, J.B.; Cen, S.; Li, Z.; Li, C.F. An unsymmetric 8-node hexahedral solid-shell element with high distortion tolerance: Linear formulations. *Int. J. Numer. Methods Eng.* **2018**, *116*, 759–783. [CrossRef]
6. Brink, U.; Stein, E. On some mixed finite element methods for incompressible and nearly incompressible finite elasticity. *Comput. Mech.* **1996**, *19*, 105–119. [CrossRef]
7. Zeng, W.; Liu, G.R. Smoothed Finite Element Methods (S-FEM): An Overview and Recent Developments. *Arch. Comput. Methods Eng.* **2018**, *25*, 397–435. [CrossRef]
8. Karabelas, E.; Haase, G.; Plank, G.; Augustin, C.M. Versatile stabilized finite element formulations for nearly and fully incompressible solid mechanics. *Comput. Mech.* **2020**, *65*, 193–215. [CrossRef]
9. Doll, S.; Schweizerhof, K.; Hauptmann, R.; Freischläger, C. On volumetric locking of low order solid and solid shell elements for finite elasto-viscoplastic deformations and selective reduced integration. *Eng. Comput.* **2000**, *17*, 874–902. [CrossRef]
10. Boffi, D.; Stenberg, R. A remark on finite element schemes for nearly incompressible elasticity. *Comput. Math. Appl.* **2017**, *74*, 2047–2055. [CrossRef]
11. Gültekin, O.; Dal, H.; Holzapfel, G.A. On the quasi-incompressible finite element analysis of anisotropic hyperelastic materials. *Comput. Mech.* **2019**, *63*, 443–453. [CrossRef]
12. Jarak, T.; Jalušić, B.; Sorić, J. Mixed Meshless Local Petrov-Galerkin Methods for Solving Linear Fourth-Order Differential Equations. *Trans. FAMENA* **2020**, *44*, 1–12. [CrossRef]
13. Guo, H.; Xiey, C.; Zhao, R. Super-convergent gradient recovery for virtual element methods. *Math. Model. Methods Appl. Sci.* **2018**, *29*, 2007–2031. [CrossRef]
14. Kaveh, A.; Seddighian, M.R. A New Nodal Stress Recovery Technique in Finite Element Method Using Colliding Bodies Optimization Algorithm. *Period. Polytech. Civ. Eng.* **2019**, *63*, 1159–1170. [CrossRef]
15. Khan, A.; Powell, C.; Silvester, D. Robust a posteriori error estimators for mixed approximation of nearly incompressible elasticity. *Int. J. Numer. Methods Eng.* **2019**, *119*, 18–27. [CrossRef]
16. Popișter, F.; Popescu, D.; Păcurar, A.; Păcurar, R. Mathematical Approach in Complex Surfaces Toolpaths. *Mathematics* **2021**, *9*, 1360. [CrossRef]
17. Gratsch, T.; Bathe, K. A posteriori error estimation technique in practical finite element analysis. *Comput. Struct.* **2005**, *83*, 75–90. [CrossRef]
18. Alshoaibi, A.M.; Bashiri, A.H. Adaptive Finite Element Modeling of Linear Elastic Fatigue Crack Growth. *Materials* **2022**, *15*, 7632. [CrossRef] [PubMed]
19. Ma, X.; Zhou, B.; Li, Y.; Xue, S. A Hermite interpolation element-free Galerkin method for elasticity problems. *J. Mech. Mater. Struct.* **2022**, *17*, 75–95. [CrossRef]
20. Vogl, C.J.; Joseph, I.; Holec, M. Mesh Refinement for Anisotropic Diffusion in Magnetized Plasmas. *arXiv* **2022**, arXiv:2210.16442. [CrossRef]
21. Saikia, B.B.; Nath, D.; Gautam, S.S. Application of machine learning in efficient stress recovery in finite element analysis. *Mater. Today Proc.* **2022**, *in press*. [CrossRef]
22. Karvonen, T.; Cirak, F.; Girolami, M. Error Analysis for a Statistical Finite Element Method. *arXiv* **2022**, arXiv:2201.07543. [CrossRef]
23. Ahmed, M. A Comparative Study of Mesh-Free Radial Point Interpolation Method and Moving Least Squares Method-Based Error Estimation in Elastic Finite Element Analysis. *Arab. J. Sci. Eng.* **2020**, *45*, 3541–3557. [CrossRef]
24. Gong, J.; Zou, D.; Kong, X.; Qu, Y.; Zhou, Y. A Non-Matching Nodes Interface Model with Radial Interpolation Function for Simulating 2D Soil–Structure Interface Behaviors. *Int. J. Comput. Methods* **2020**, *18*, 2050023. [CrossRef]
25. Cao, Y.; Yao, L.; Yin, Y. New treatment of essential boundary conditions in EFG method by coupling with RPIM. *Acta Mech. Solida Sin.* **2013**, *26*, 302–316. [CrossRef]
26. Ahmed, M.; Singh, D. An adaptive parametric study on mesh refinement during adaptive finite element simulation of sheet forming operations. *Turk. J. Eng. Environ. Sci.* **2008**, *13*, 163–175.
27. Liu, G.R.; Gu, Y.T. A local radial point interpolation method (LR-PIM) for free vibration analyses of 2-D solids. *J. Sound Vib.* **2001**, *246*, 29–46. [CrossRef]
28. Wang, J.; Liu, G.R. A point interpolation meshless method based on radial basis functions. *Int. J. Numer. Methods Eng.* **2002**, *54*, 1623–1648. [CrossRef]

29. Wang, J.; Liu, G. On the optimal shape parameters of radial basis functions used for 2-D meshless methods. *Comput. Methods Appl. Mech. Eng.* **2002**, *191*, 2611–2630. [CrossRef]
30. Zienkiewicz, O.C.; Lui, Y.C.; Huang, G.C. Error Estimates and convergence rate for various incompressible elements. *Int. J. Numer. Methods Eng.* **1989**, *28*, 2192–2202. [CrossRef]
31. Onate, E.; Perazzo, F.; Miquel, J. A finite point method for elasticity problems. *Comput. Struct.* **2001**, *79*, 2151–2163. [CrossRef]
32. Li, X.D.; Wiberg, N.E. A posteriori Error Estimate by Element Patch Post-processing, Adaptive Analysis in Energy and L_2 Norms. *Comp. Struct.* **1994**, *53*, 907–919. [CrossRef]